PLANT SYMBIOSIS

Receptor-associated kinases control the lipid provisioning program in plant–fungal symbiosis

Sergey Ivanov and Maria J. Harrison*

The mutualistic association between plants and arbuscular mycorrhizal (AM) fungi requires intracellular accommodation of the fungal symbiont and maintenance by means of lipid provisioning. Symbiosis signaling through lysin motif (LysM) receptor-like kinases and a leucine-rich repeat receptor-like kinase DOES NOT MAKE INFECTIONS 2 (DMI2) activates transcriptional programs that underlie fungal passage through the epidermis and accommodation in cortical cells. We show that two *Medicago truncatula* cortical cell–specific, membrane-bound proteins of a CYCLIN-DEPENDENT KINASE-LIKE (CKL) family associate with, and are phosphorylation substrates of, DMI2 and a subset of the LysM receptor kinases. *CKL1* and *CKL2* are required for AM symbiosis and control expression of transcription factors that regulate part of the lipid provisioning program. Onset of lipid provisioning is coupled with arbuscule branching and with the REDUCED ARBUSCULAR MYCORRHIZA 1 (RAM1) regulon for complete endosymbiont accommodation.

Arbuscular mycorrhizal (AM) symbioses are widespread in terrestrial environments; they influence plant mineral nutrition and carbon allocation below ground and, consequently, ecosystem productivity (*1*). The endosymbiosis develops in the roots, where differentiated hyphae called arbuscules are accommodated in membrane-bound apoplastic compartments generated de novo within the cortical cells (*2*, *3*). These elaborate interfaces are the sites of nutrient exchange. The mutualism requires substantial modifications to root cell metabolism and transport to enable the cell to provision the lipid auxotrophic endosymbiont and to access the phospha delivers (*4*). These modifications are achi through alterations to the root cortical cell transcriptome, but knowledge of the signaling that underlies these responses is still incomplete.

AM symbiosis arose early in the plant lineage (*5*), and AM symbiosis–competent host plants share several genes conserved in hosts and missing from nonhosts (*6*, *7*). These so-called AM symbiosis–conserved genes include a family of kinases that cluster within a larger family referred to as *CYCLIN-DEPENDENT KINASE-LIKE* (*CKL*) (*6*, *8*). The genome of model plant *Medicago truncatula* (*Medicago*) contains two AM symbiosis–conserved *CKL* genes, which we refer to as *CKL1* and *CKL2*. The *CKL* family is related to but distinct from the canonical cyclin-dependent kinases (fig. S1, A and B). To date, functions for *CKL* family members have not been reported.

CKL1 and *CKL2* are required for expression of part of the lipid provisioning program

Expression of *CKL1* and *CKL2* is induced during AM symbiosis (fig. S1C), and the promoters of

Boyce Thompson Institute, Ithaca, NY 14853, USA.
*Corresponding author. Email: mjh78@cornell.edu

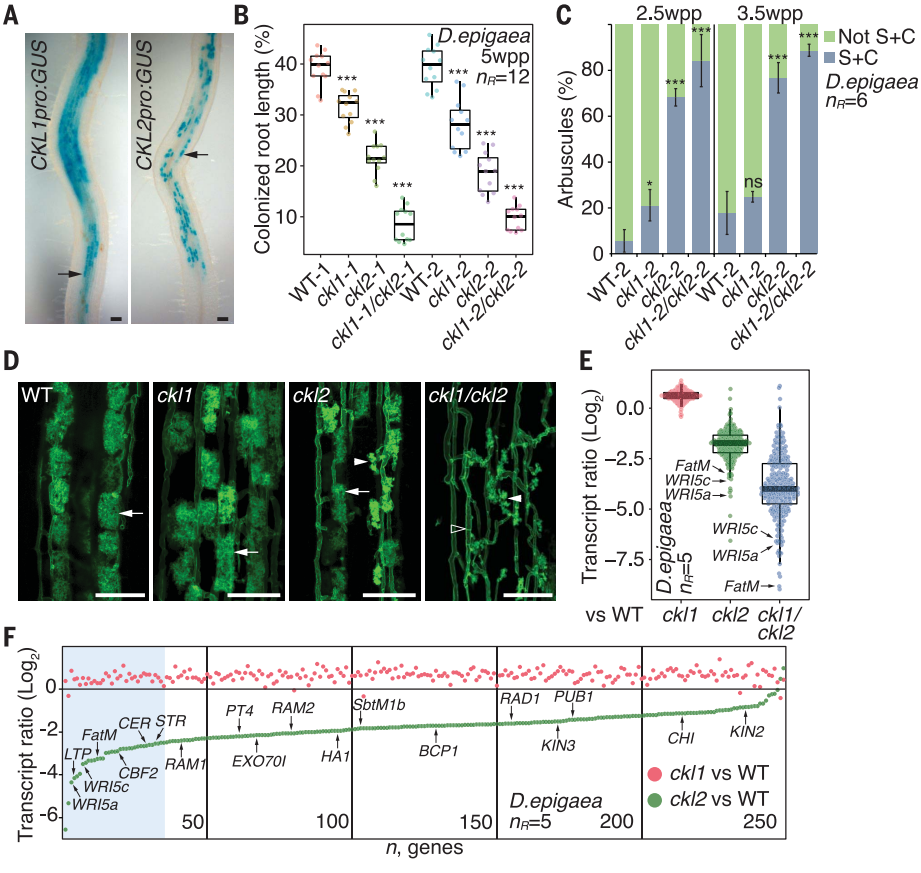

Fig. 1. *CKL1* and *CKL2* are required for AM symbiosis. (**A**) *CKL1* and *CKL2* promoter activity in *M. truncatula* roots colonized by AM fungus *Rhizophagus irregularis* as assessed through β-glucuronidase (GUS) activity. Arrows indicate arbuscules. Scale bars, 100 μm. (**B** to **F**) Effect of mutations in *CKL1* and *CKL2*. (B) The percentage of root length with intraradical colonization in WT segregant (WT), *ckl1*, *ckl2*, and *ckl1/ckl2* mutants colonized by AM fungus *D. epigaea* 5 weeks postplanting (wpp). n_R = 12, number of root systems evaluated for each mutant allele (***P < 0.001; ns, not significant; t test). (C) Proportion of senescing and collapsed arbuscules (S+C) and not senescent or collapsed arbuscules (Not S+C) in WT segregants, *ckl1*, *ckl2*, and *ckl1/ckl2* (*P < 0.01; ***P < 0.001; t test). (D) Arbuscules in WT, *ckl1*, *ckl2*, and *ckl1/ckl2*. Confocal microscopy images of WT and mutant roots stained with wheat germ agglutinin (WGA)–Alexa488 to visualize fungal structures (z-stack projection, n = 10 optical slices, 1-μm intervals). Arrows indicate mature arbuscules; solid arrowheads indicate senescing and collapsed arbuscules; open arrowhead indicates fungal septa. Scale bars, 100 μm. (E) Box plot shows transcript ratios (log_2) in colonized roots *ckl1*:WT, *ckl2*:WT, and *ckl1/ckl2*:WT. Box plot shows median, upper, and lower quartiles, and whiskers show 1.5 interquartile range. (F) Transcript ratios, *ckl1*:WT and *ckl2*:WT, from colonized roots in rank order based on *ckl2*:WT data. Blue shading shows the 15th percentile. Lipid provisioning–related genes and AM marker genes are indicated. Data in (E) and (F) are the top 250 genes induced in *D. epigaea*–colonized WT relative to mock-inoculated control (fig. S5A). Experiments were replicated as shown in table S8.

both genes are active in the cortex of roots colonized by AM fungi (Fig. 1A and fig. S1D). *CKL2* promoter activity is restricted to colonized cells containing arbuscules, whereas the *CKL1* promoter is active in colonized and adjacent non-colonized cells (Fig. 1A and fig. S1D). Constitutive expression of gain-of-function variants of the major regulators *DOES NOT MAKE INFECTIONS 3* (*DMI3*) (*9*) and *DELLA* (*10*), but not *REDUCED ARBUSCULAR MYCORRHIZA 1* (*RAM1*) (*11*), drives 10- to 100-fold increases in *CKL1* and *CKL2* transcripts in uninoculated roots (fig. S1, E to G). These data indicate differences in the control of *CKL* expression relative to genes of the accommodation program (*12*). Public transcriptome data indicate almost AM symbiosis–specific expression of *CKL2*, whereas *CKL1* expression is detected in non-AM symbiotic conditions (fig. S2).

To assess *CKL1* and *CKL2* functions during AM symbiosis, we generated *Medicago* mutants using CRISPR-Cas9 genome editing and obtained two independent alleles for each gene and two corresponding double mutants. The mutations resulted in premature stop codons (fig. S3A and table S1). The *ckl* mutants did not exhibit visible differences in general root or shoot growth relative to the wild-type (WT) segregants (fig. S3B). After inoculation with AM fungus *Diversispora epigaea*, initial hyphal penetration of the epidermis was equivalent in mutants and WT (fig. S3, C and D), but intraradical colonization was impaired in the mutants (Fig. 1B). Relative to WT, *ckl1* alleles showed, on average, a 24% reduction in fungal colonized root length, whereas *ckl2* and the *ckl1/ckl2* alleles showed, on average, a 49 and 77% reduction in fungal colonized root length, respectively (Fig. 1B). In addition, *ckl2* and *ckl1/ckl2* showed more than 60 and 80% senescing and collapsed arbuscules, respectively (Fig. 1, C and D, and fig. S3E). Periarbuscular membrane (PAM)–resident proteins PHOSPHATE TRANSPORTER 4 (PT4) (*13*) and BLUE COPPER BINDING PROTEIN 1 (BCP1) (*14*), as well as members of symbiotic exocytotic membrane fusion machinery, could be detected in *ckl2* and *ckl1/ckl2* mutants, indicating that PAM development and trafficking of proteins occur in the mutants before arbuscule collapse (fig. S3, F and G). Endoreduplication occur in AM roots and results in measurable increases in nuclei size in colonized cortical cells (*15*). The size of nuclei in WT and *ckl1/ckl2* colonized cells did not differ, thus falsifying an initial hypothesis that *CKL1* and *CKL2* are required for cortical cell endoreduplication during symbiosis (fig. S4).

We examined the transcript profiles of *ckl* mutant roots with and without colonization by *D. epigaea* (Fig. 1, E and F; fig. S5; and data S1). Transcript profiles of *ckl1* and WT colonized roots were similar to each other and showed the expected marker gene expression (*16*). More than 250 genes showed a $\log_2$-fold increase of >2, and 165 genes showed a $\log_2$-fold increase of >5 in transcript level in colonized roots relative to mock-inoculated controls. Transcriptional increases in marker genes in colonized *ckl2* and *ckl1/ckl2* roots were lower than those of WT and *ckl1*, which is consistent with lower levels of fungal colonization (fig. S5B). Examination of *ckl2*:WT transcript ratios from colonized roots revealed a small group of genes expressed at very low levels in *ckl2* (Fig. 1, E and F, and data S1). This group included genes with essential roles in AM symbiosis including *WRINKLED* transcription factors *WRI5a* and *WRI5c* (*17*, *18*), as well as *FATTY ACYL-ACP THIOESTERASE M* (*FatM*) and *STUNTED ARBUSCULE* (*STR*) (*19*, *20*), which are regulated by WRI5a and WRI5c (*18*). The *ckl1/ckl2*:WT transcript ratios showed a similar pattern to that observed for *ckl2*:WT, with a slightly different rank order (fig. S5C). FatM is required for fatty acid biosynthesis, and STR, a half-size ABC transporter (*20*), is involved in lipid export to the fungus (*17*, *19*–*22*); their loss-of-function phenotypes are similar to those of *ckl2* and *ckl1/ckl2* mutants. At least two other genes in the *ckl2* low-expression group have predicted lipid-related roles, including a lipid transfer protein (*LTP*) and a ceramidase (*CER*) (Fig. 1F and data S1); however, *RAM2*, a glyceraldehyde-3-phosphate acyltransferase, also essential in the lipid biosynthesis program but directly regulated by *RAM1* (*11*, *17*), was not in this group. Although any of the genes in the low-expression cluster could contribute to the *ckl2* mycorrhizal phenotype, reduced expression of *WRI5a*, *WRI5c*, *FatM*, and *STR* alone is sufficient to explain the *ckl2* and *ckl1/ckl2* mutant phenotypes. Thus, we conclude that *CKL1* and *CKL2* functions are necessary for expression of several genes

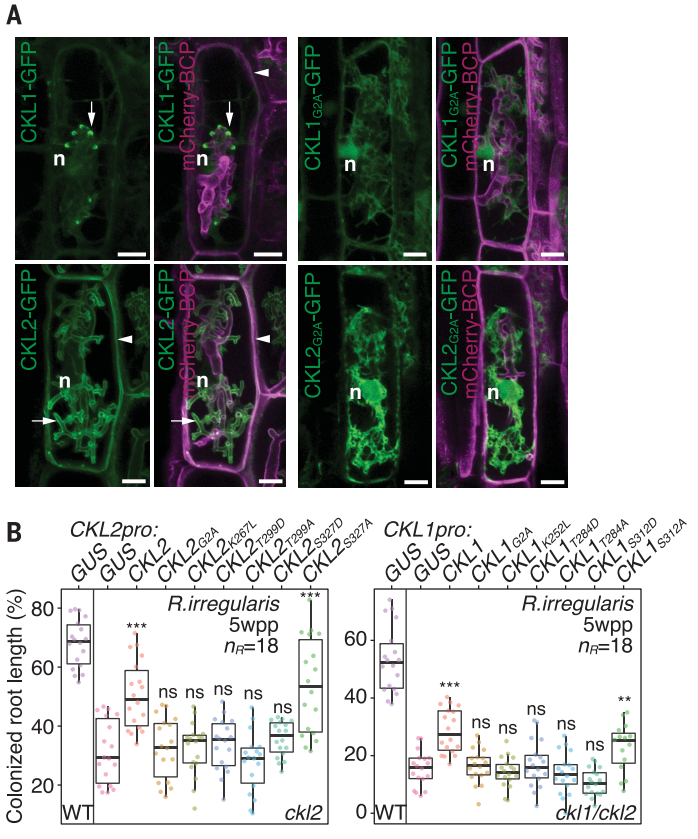

Fig. 2. CKL1 and CKL2 functions require membrane location and kinase activity. (**A**) CKL1 and CKL2 fusion proteins expressed from their native promoters. CKL1-GFP detected on the PAM in the region around the tips of arbuscule branches (arrow). CKL2-GFP detected on the PAM (arrow) and PM (arrowhead). Myristoylation mutants $CKL1_{G2A}$-GFP and $CKL2_{G2A}$-GFP lost their membrane association and located in the cytoplasm and nucleoplasm. Proteins were coexpressed with a PM and PAM marker (mCherry-BCP). Confocal microscopy images (z-stack projection, n = 10 optical slices, 0.5-μm intervals). n, nucleus. Scale bars, 10 μm. (**B**) Complementation of colonization in *ckl2* or *ckl1/ckl2* with different CKL1 and CKL2 variants, including myristoylation mutant ($CKL1_{G2A}$ and $CKL2_{G2A}$), kinase active site mutant ($CKL1_{K252L}$ and $CKL2_{K267L}$; fig. S1B), phosphoablative ($CKL1_{T284A}$ and $CKL2_{T299A}$) and phosphomimetic ($CKL1_{T284D}$ and $CKL2_{T299D}$) mutants of the conserved threonine in kinase domain activation segment (fig. S1B), and phosphoablative ($CKL1_{S312A}$ and $CKL2_{S327A}$) and phosphomimetic ($CKL1_{S312A}$ and $CKL2_{S327A}$) mutants of a conserved serine. Percentage of root length with intraradical colonization by *R. irregularis* at 5 wpp, n_R = 12, number of evaluated root systems for each mutant. WT included for colonization reference. Asterisks indicate the level of statistical significance (**P < 0.01; ***P < 0.001; t test) in comparison to mutants expressing a GUS gene from the CKL1 or CKL2 promoters. The *ckl1/ckl2* mutant provided a sensitized background against which to assess the *CKL1* variants. Experiments were replicated as shown in table S8.

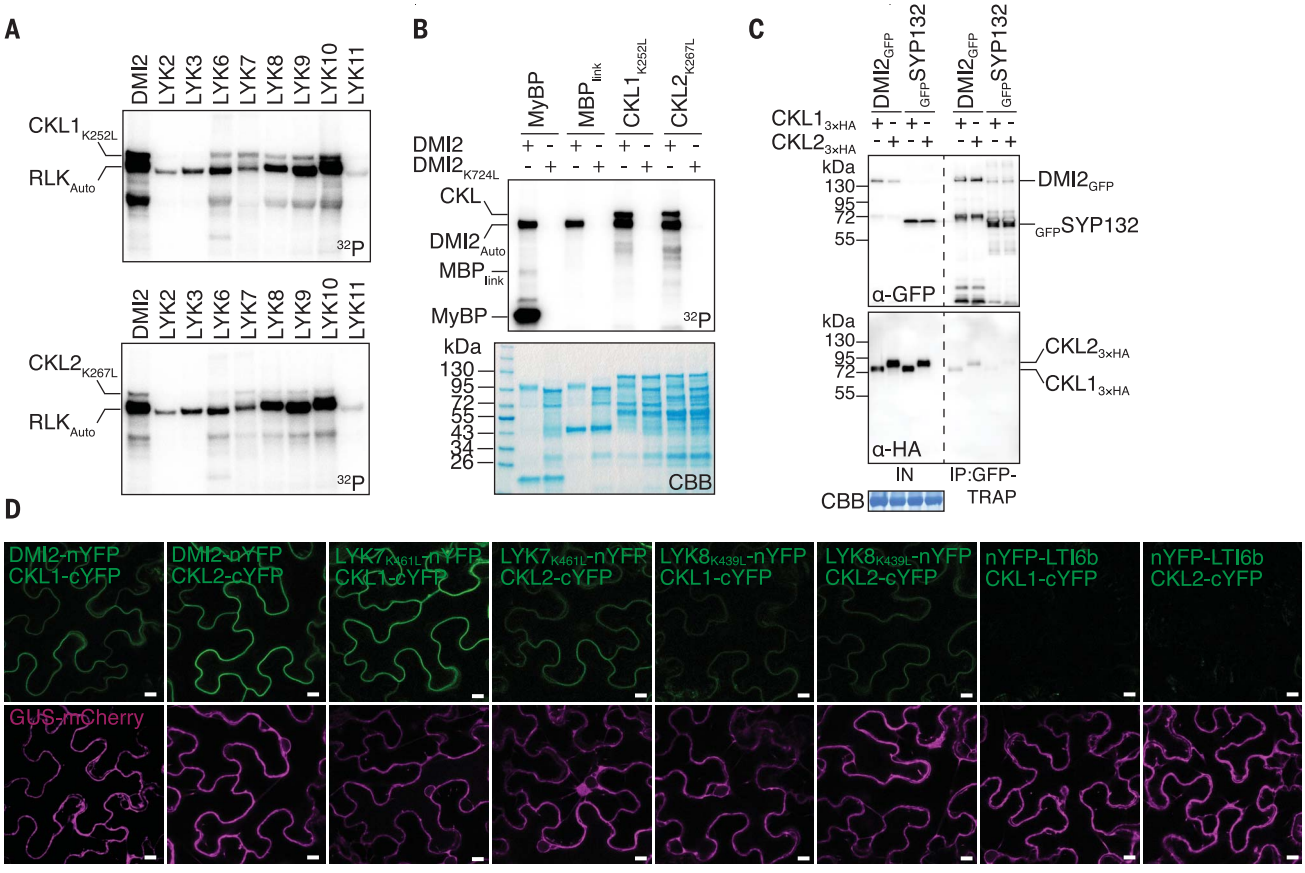

Fig. 3. DMI2 and a subset of the LysM-RLKs interact with, and phosphorylate, CKL1 and CKL2. (**A** and **B**) ^{32}P radiographs showing in vitro transphosphorylation of kinase-dead $CKL1_{K252L}$ and $CKL2_{K267L}$ by RLKs (endodomains) (A); phosphorylation is abolished when kinase-dead $DMI2_{K724L}$ is used (B). Myelin basic protein (MyBP) was used as generic phosphorylation substrate. The kinases were purified as maltose binding protein (6×His-MBP) fusions, so free maltose binding protein with recombination linker (MBP_{link}) was included as a negative control. RLK_{Auto}, autophosphorylation of RLKs; CBB, Coomassie brilliant blue stained gel corresponds to radiograph in (B). (**C**) Coimmunoprecipitation assay of $CKL1_{3\times HA}$ or $CKL2_{3\times HA}$ with DMI2-GFP. GFP-SYP132 was used as a membrane protein control for immunoprecipitation. Western blots were probed with antibodies α-GFP and α-HA. IN, input; IP, immunoprecipitation. (**D**) BiFC assays of CKL1-cYFP or CKL2-cYFP and RLKs-nYFP in *N. benthamiana* leaves. YFP complementation is visualized in transformed cells that exhibit fluorescence from transformation marker GUS-mCherry. nYFP-LTI6b serves as a membrane protein negative control. *CKL1-cYFP* or *CKL2-cYFP* (fusions to C-terminal fragment of YFP) and *DMI2-nYFP* or kinase-dead variants *LYK7$_{K461L}$-nYFP*, *LYK8$_{K439L}$-nYFP*, or *nYFP-LTI6b* (fused to N-terminal fragment of YFP) were expressed from a single transfer DNA with *GUS-mCherry*. Confocal microscopy images. Scale bars, 10 μm. Experiments were replicated as shown in table S8.

involved in the production and provisioning of lipids to the fungus.

Membrane association and kinase activity are required for CKL1 and CKL2 functions

The subcellular location of each CKL protein was assessed through visualization of translational fusions with fluorescent proteins expressed from the native *CKL1* or *CKL2* promoters. CKL1-GFP (green fluorescent protein) was visible at the PAM in the region around the tips of arbuscule branches and in the cytoplasm and nucleoplasm, whereas CKL2-GFP showed an even distribution exclusively across the entire plasma membrane (PM) and PAM (Fig. 2A and fig. S6, A to C). Both proteins were detected throughout the arbuscule lifetime (fig. S7). The CKL proteins lack transmembrane domains, but both proteins are predicted to be myristoylated. Mutation of the myristoylation motif (G2A) abolished membrane association of each CKL protein and resulted in their accumulation in the cytoplasm and nucleoplasm (Fig. 2A and fig. S6D).

Using in vitro phosphorylation assays, we found that CKL1 and CKL2 were capable of autophosphorylation and transphosphorylation of a generic substrate, myelin basic protein. Phosphorylation activity was abolished by mutation of the predicted kinase active site, $CKL1_{K252L}$ and $CKL2_{K267L}$ (K, Lys; L, Leu; figs. S1B and S8A). *CKL* genes encoding kinase-dead mutant proteins expressed from their native promoters failed to complement *ckl2* or *ckl1/ckl2* mutants (Fig. 2B). Likewise, *CKL1* and *CKL2* myristoylation motif mutants were also unable to restore colonization in *ckl1/ckl2* (Fig. 2B and fig. S9). Thus, CKL1 and CKL2 kinase activities and membrane location are essential for their functions.

CKL proteins are phosphorylated by two classes of receptor-like kinases that function during AM symbiosis

Given their locations at the PM and PAM and their downstream impact on transcription, we hypothesized that CKL1 and CKL2 might be involved in signal transduction from membrane receptor kinases. Members of two classes of receptor-like kinases (RLKs) are central to AM symbiosis signaling: the lysin motif (LysM) receptor-like kinases (*23*–*25*) and a malectin-like domain and leucine-rich repeat (MLD-LRR) receptor-like kinase, DMI2 (*Lotus japonicus SYMRK*) (*26*, *27*). During AM symbiosis, chitooligosaccharides are perceived by LysM-RLKs, and, in the presence of DMI2, symbiosis signaling is initiated. This leads to nuclear calcium oscillations and expression of genes for intracellular accommodation of the AM fungus (*23*, *28*, *29*). The mechanisms

underlying signal transduction from membrane-located RLKs to the nucleus are unclear but may involve a metabolite, mevalonate (*30*). Chitooligosaccharide signaling has been studied mostly in epidermal cells but is proposed to occur also in cortical cells coincident with fungal colonization of the root cortex (*31*). Consistent with this proposal, we detected promoter activity of *DMI2* and several *LysM-RLKs* in cortical cells, although DMI2-GFP and LysM-RLK-GFP protein fusions were below our limits of detection (fig. S10). To determine whether DMI2 or LysM-RLKs could phosphorylate CKL1 or CKL2, the endodomains of DMI2 and 10 *Medicago* LysM-RLKs (LYK2 to LYK11) (table S1) were purified, and their kinase activity was evaluated using in vitro phosphorylation assays (fig. S8, C and D). $CKL1_{K252L}$ and $CKL2_{K267L}$ protein variants, which lack kinase activity, were provided as substrates to enable an assessment of transphosphorylation by the RLKs. DMI2 and five LysM-RLKs (LYK6 to LYK10) phosphorylated CKL1 and CKL2, whereas phosphorylation was not detected for three LysM-RLKs (LYK2, LYK3, and LYK11) (Fig. 3, A and B, and fig. S11, A and B). LYK3, an RLK generally considered specific for Nod factor signaling (*32*), shows autophosphorylation activity comparable to, if not higher than, that of LYK7 but no phosphorylation of $CKL1_{K252L}$ or $CKL2_{K267L}$. Thus, these data suggest some selectivity among these RLKs for CKL substrates. The CKLs each contain many potential phosphorylation sites; in an initial assay with fragments of the CKL proteins, DMI2 preferentially phosphorylated the C-terminal regions of $CKL1_{K252L}$ and $CKL2_{K267L}$ (fig. S11C). CKL1 and CKL2 were evaluated for their ability to phosphorylate kinase-dead variants of DMI2, LYK2 to LYK11, and LYK-related (LYR) co-receptors, LYR1, LYR4, LYR8, and NOD FACTOR PERCEPTION (NFP) (fig. S8B). Neither CKL1 nor CKL2 phosphorylated these RLK endodomains (fig. S12). Thus, data from in vitro kinase assays support the hypothesis that CKL1 and CKL2 are phosphorylation substrates of DMI2 and a subset of the LysM-RLKs.

To assess association of CKL1 and CKL2 with the RLKs, genes encoding full-length *CKL1* or *CKL2* epitope-tagged fusions were transiently coexpressed with full-length *DMI2-GFP*, *LYK3-GFP*, *LYK9-GFP*, *LYK10-GFP*, *NFP-GFP*, or *LYR1-GFP* in *Nicotiana benthamiana* leaves (fig. S13A) and interactions assessed using coimmunoprecipitation assays from cell extracts. $CKL1_{3\times HA}$ and $CKL2_{3\times HA}$ coimmunoprecipitated with DMI2-GFP, indicating their associations in planta (HA, hemagglutinin; Fig. 3C and fig. S13B). In addition, $CKL1_{3\times HA}$ and $CKL2_{3\times HA}$ coimmunoprecipitated with LYR1-GFP, an inactive LysM-RLK (fig. S13C), and to a lesser extent with LYK3, LYK9, and LYK10 (fig. S13C). Expression of *LYK9-GFP* in *N. benthamiana* leaves induces cell death (*23*), which compromises the coimmunoprecipitation assays. A similar response, even stronger than that elicited by LYK9, was observed for *LYK7-GFP* and *LYK8-GFP* (fig. S13D). Cell death was not induced by the kinase-dead variants $LYK7_{K461L}$, $LYK8_{K439L}$, or $LYK9_{K443L}$ (fig. S13D). Both $LYK7_{K461L}$-GFP and $LYK8_{K439L}$-GFP accumulated in the PM (fig. S13E); however, $LYK9_{K443L}$-GFP lost its membrane location and accumulated in the cytosol (fig. S13E). Kinase-dead LYK7 and LYK8 variants offer an opportunity to assess interactions with CKL proteins. In coimmunoprecipitation assays, $CKL1_{3\times HA}$ and $CKL2_{3\times HA}$ coimmunoprecipitated with $LYK7_{K461L}$-GFP and $LYK8_{K439L}$-GFP (fig. S13F). Trace amounts of CKL were visible in some of the MtLTI6b and MtSYP132 coimmunoprecipitation negative controls, albeit at levels lower than the RLK coimmunoprecipitations (Fig. 3C and fig. S13, B and F). Therefore, to further evaluate CKL–RLK interactions, we implemented bimolecular fluorescence complementation (BiFC) assays using proteins tagged with N-terminal (nYFP) or C-terminal (cYFP) fragments of yellow fluorescent protein. DMI2-nYFP interacted with CKL1-cYFP and CKL2-cYFP in BiFC assays and did not interact with the LTI6b membrane protein control (Fig. 3D). Interactions of CKL proteins with $LYK7_{K461L}$-nYFP and $LYK8_{K439L}$-nYFP were also detected (Fig. 3D), whereas interactions with the cytosol-located $LYK9_{K443L}$ were not detected (fig. S14A). Interactions between CKL proteins and LYK10 or LYR1 were not visible; however, a weak fluorescence complementation signal for LYK10 with CKL2 was detected when coexpressed with LYR1 (fig. S14B), suggesting that the predicted co-receptor may stabilize this interaction. As anticipated, given the cell death responses, interactions between active LYK7, LYK8, or LYK9 and CKLs were not detected by BiFC assays (fig. S14C). On the basis of these data, we conclude that CKL1 and CKL2 each interact with DMI2 and at least two LysM-RLKs, LYK7 and LYK8. Together, the interaction data and the finding that DMI2 and LYK6 to LYK10 phosphorylate CKL1 and CKL2 support the hypothesis that CKL1 and CKL2 are substrates for RLK signal transduction.

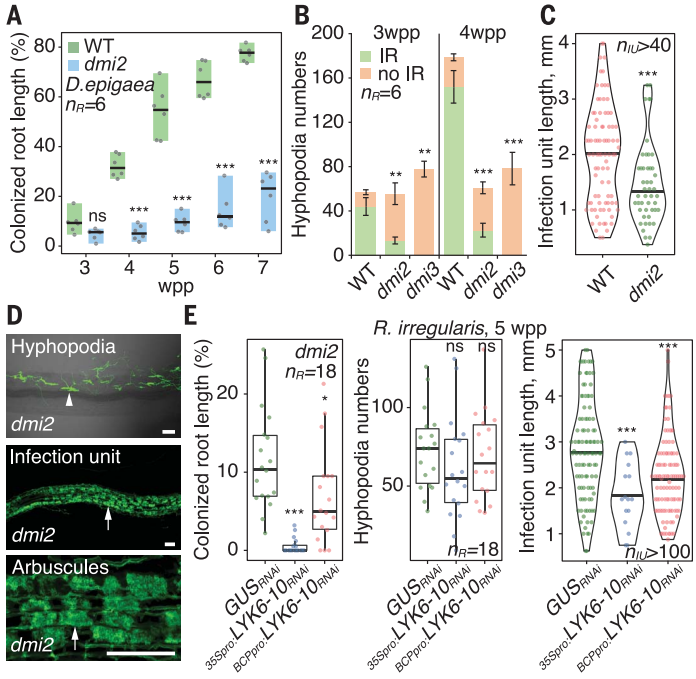

Fig. 4. DMI2 and LysM-RLKs contribute to intraradical colonization. (**A**) Limited intraradical colonization in *dmi2-7* relative to WT. n_R = 6 root systems per genotype at each time point. (**B**) Hyphopodia that penetrate the epidermis and result in intraradical colonization (IR) or fail to penetrate and lack intraradical colonization (no IR) in WT A17, *dmi2-7*, and *dmi3* (TRV25) at 3 and 4 wpp. Error bars are standard errors. (**C**) Infection unit (IU) length is shorter in *dmi2-7* relative to WT. n_{IU} > 40, number of infection units measured at 3 wpp (**P < 0.01; ***P < 0.001; t test). (**D**) Most hyphopodia fail to penetrate the epidermis (as indicated by the arrowhead). A few successful penetrations lead to intraradical colonization with arbuscules (arrow) in *dmi2-7*. Confocal microscopy images of roots stained with WGA-Alexa488 to visualize fungal structures (z-stack projection, n = 10 of optical slices, 1-μm interval). Scale bars, 100 μm. (**E**) A subset of the LysM-RLKs are required for expansion of intraradical infection units in *dmi2-7*. Effect of an RNAi construct ($LYK6\text{-}10_{RNAi}$) targeting LYK6, LYK7, LYK8, LYK9, and LYK10 expressed from constitutive *CaMV35S* promoter (*35Spro*) or symbiosis-induced, cortical cell–specific BCP1 promoter (*BCP1pro*) on the percentage of root length with intraradical colonization, number of hyphopodia, and length of infection units in *dmi2-7* at 5 wpp. Comparison made to *dmi2-7* expressing a GUS-RNAi vector control (*P < 0.05; ***P < 0.001; t test). Experiments were replicated as shown in table S8.

DMI2 and LysM-RLKs are required to support fungal colonization in the cortex

The *Medicago* LysM-RLK gene family is large, and it is likely that its members show some

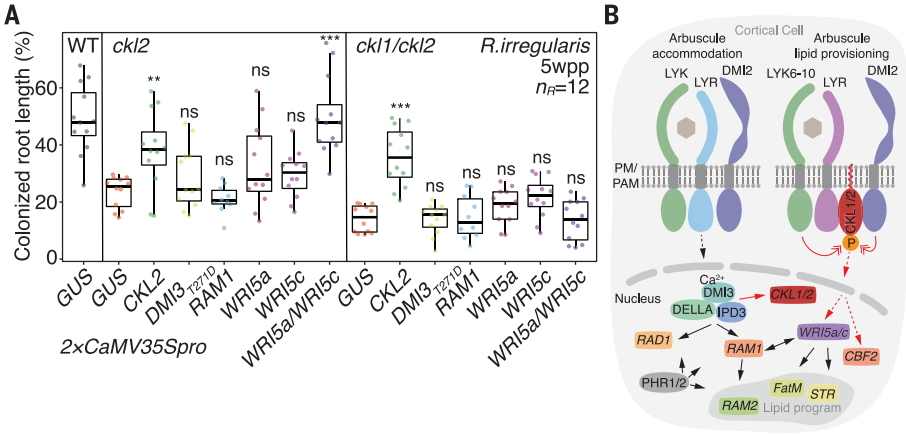

Fig. 5. CKL1 and CKL2 are components of a signaling pathway regulating the lipid provisioning program. (**A**) Simultaneous overexpression (double *CaMV35S* promoter, *2×CaMV35Spro*) of *WRI5a* and *WRI5c*, but not gain-of-function $DMI3_{T271D}$, *RAM1*, *WRI5a*, or *WRI5c*, increases intraradical colonization in *ckl2* but not in *ckl1/ckl2*. *2×CaMV35Spro:CKL2* serves as a positive complementation control and *2×CaMV35Spro:GUS* as a vector control. n_R = 12, number of evaluated transgenic root systems for each transformation (**P < 0.01; ***P < 0.001; t test). (**B**) Proposed model of CKL1 and CKL2 action. In cortical cells, initial signaling by LysM-RLKs (LYK-LYR complex) in concert with DMI2 leads to the activation of a nuclear-located DMI3-IPD3 complex, which along with DELLA induces expression of *CKL1* and *CKL2* and the transcriptional regulators *RAM1* and *RAD1*. The RAM1 regulon includes *RAM2* and, either directly or indirectly, genes involved in intracellular accommodation functions including generation of the PAM. Upon location at the PM and PAM, CKL1 and CKL2 proteins are phosphorylated by DMI2 and a subset of LysM-RLKs and transduce signaling, which ultimately leads to the transcriptional activation of several transcriptional regulators, including *WRI5a* and *WRI5c* and downstream target genes *FatM* and *STR*. The CKL1/2 signaling pathway controls the onset of the lipid provisioning program. Feedback regulation of *RAM1* by WRI5s (*16*) may further amplify the cellular accommodation pathway, including expression of *RAM2*. PHOSPHATE STARVATION RESPONSE 1 and 2 (PHR1/2) promote expression of most symbiosis-associated genes (*43*, *44*). Black solid arrows and red solid arrows indicate transcriptional regulation and refer to data published previously (black) (*9*, *12*, *27*, *40*–*44*) or presented here (red). Red double-headed arrow indicates phosphorylation. Red dashed arrow indicates unknown intermediate components.

level of functional redundancy (*33*). *Medicago lyk9* displays a modest quantitative reduction in AM fungal colonization relative to WT, and a further reduction is observed in a *lyk9/nfp* double mutant (*23*, *34*). By contrast, *dmi2* shows a strong AM symbiosis phenotype. *DMI2* and *Lotus japonicus* ortholog, *SYMRK*, are required for efficient hyphal entry through the epidermis (*27*, *35*), and most studies have focused on this epidermal function. However, occasional colonization of the root cortex has been reported in *symrk* alleles (*36*, *37*). In Medicago, *DMI2* is also required to support intraradical colonization of the cortex; colonized root lengths of *dmi2-7* and WT are similar at 3 weeks after planting, but by 7 weeks after planting, colonization levels in *dmi2-7* are <25% those of WT (Fig. 4, A and B). At 3 weeks after planting, individual infection units in *dmi2-7* are 37.5% shorter than those in WT, indicating that loss of DMI2 slows fungal growth in the cortex (Fig. 4C). Arbuscules show a WT appearance, and PT4 is present on PAM, indicating normal trafficking and PAM development in *dmi2-7* (Fig. 4D and fig. S15A), which suggest that the slower intraradical fungal growth is not the result of an impaired symbiotic interface. Slower growth could, however, result from a partial reduction in lipid provisioning. Expression of *DMI2* from an AM symbiosis–induced, cortical cell–specific promoter (*BCP1*) promotes fungal colonization in *dmi2-7* roots, further supporting a role for *DMI2* in the cortex (fig. S15B). *DMI2* is also required for symbiosis with nitrogen-fixing bacteria, where, similar to our current observations, the protein functions in both epidermal and cortical cells (*38*).

The mycorrhizal phenotypes of *ckl2* and *ckl1/ckl2* are considerably more severe than those of the RLK mutants; the differences in phenotypic severity could be explained if the CKLs integrate signals from both LysM-RLKs and DMI2. Expression of an RNA interference (RNAi) construct targeting LysM-RLKs *LYK6*, *LYK7*, *LYK8*, *LYK9*, and *LYK10* simultaneously from either the *CaMV35S* or the *BCP1* promoters did not affect hyphopodia numbers on the epidermis but did decrease total colonization and infection unit length in *dmi2-7*, indicating an additive effect of these RLKs on cortical colonization (Fig. 4E and fig. S15C). These data are consistent with the hypothesis of signal integration potentially at the CKLs. To provide further support that CKLs act downstream of DMI2 and the LysM-RLKs, we attempted to generate constitutively active CKL kinases. However, for both CKL1 and CKL2, mutation of the conserved threonine in the activation segment ($CKL1_{T284D}$ and $CKL2_{T299D}$; T, Thr; D, Asp), which in some cases causes constitutive activation, resulted in proteins unable to complement the respective *ckl* mutants (Fig. 2B). Mutation of a serine that is conserved in CKL1 and CKL2 proteins from AM symbiosis host species ($CKL1_{S312}$ and $CKL2_{S327}$; S, Ser) resulted in CKL proteins capable of complementing their respective mutants only when the mutation was phosphoablative ($CKL1_{S312A}$ and $CKL2_{S327A}$; A, Ala). The corresponding phosphomimetic ($CKL1_{S312D}$ and $CKL2_{S327D}$) mutant proteins did not complement the *ckl* mutants, suggesting potential negative regulation of the CKLs through phosphorylation of this residue (Fig. 2B). Overexpression of both *CKL1* and *CKL2*, $CKL1_{S312A}$ and $CKL2_{S327A}$, or $CKL1_{S312D}$ and $CKL2_{S327D}$ proteins did not rescue the *dmi2-7* low-colonization phenotype (fig. S15D), consistent with the hypothesis that DMI2 activates CKL1 and CKL2. However, the absence of gain-of-function CKL1 and CKL2 variants precludes a final test of this hypothesis.

Simultaneous overexpression of two WRI5 transcription factors suppresses the *ckl2* phenotype

To determine whether signaling downstream of CKLs involves proteins of the symbiosis signaling pathway, we focused on central regulators, a calcium- and calmodulin-dependent protein kinase DMI3 (CCaMK in *L. japonicus*) (*9*), INTERACTING PROTEIN of DMI3 (IPD3; CYCLOPS in *L. japonicus*) (*39*, *40*), and transcriptional regulators RAM1 (*11*, *12*) and the WRI5s (*17*, *18*), which together regulate transcription of many cellular accommodation and lipid provisioning genes. Simultaneous overexpression of *WRI5a* and *WRI5c* suppressed *ckl2*, resulting in colonization comparable to that obtained by expressing *CKL2*, whereas overexpression of a constitutively active version of $DMI3_{T271D}$ (*41*) or *RAM1* did not suppress the *ckl2* phenotype (Fig. 5A). These data, along with the *ckl2* transcript profiles, support the hypothesis that *WRI5a* and *WRI5c* act downstream of *CKL2*. However, simultaneous overexpression of *WRI5a* and *WRI5c* was insufficient to suppress *ckl1/ckl2*, likely because additional transcriptional regulators (Fig. 1F) are required to obtain full gene expression in this double-mutant background.

In summary (Fig. 5B), we propose that initial symbiosis signaling, involving the LysM-RLKs and DMI2 proteins, leads to the expression of arbuscule accommodation genes regulated through RAM1 as described (*42*) and to the expression of the *CKL* genes via DMI3, IPD3, and DELLA. CKL proteins locate at the PM and PAM, where they associate with DMI2 and

LysM-RLKs and redirect RLK signaling through a pathway independent of DMI3 and RAM1. This ultimately leads to the transcriptional activation of several regulators, including *WRI5a* and *WRI5c* and their target genes, *FatM* and *STR* (*18*), for fatty acid biosynthesis and export. As shown previously, WRI5s also increase *RAM1* expression (*18*), and, consequently, CKL signaling has the potential to further amplify the RAM1 regulon and therefore to increase the expression of *RAM2*, another central component of the lipid provisioning pathway. Thus, the data identify roles of CKL1 and CKL2 and uncover two gene modules within the lipid provisioning program whose expression is directed by two distinct but interconnected signaling pathways. As configured, a functional lipid program, which requires *FatM*, *RAM2*, and *STR* (*17*, *19*, *21*, *22*), will be expressed only coincident with arbuscule branching and not during the cellular accommodation associated with hyphal passage through cortical cells. Such mechanisms may extend to monocots, as shown by the single AM-conserved *CKL* in *Brachypodium distachyon*, whose loss-of-function phenotype, protein location at the PAM and PM, and interaction with BdDMI2 (fig. S16) mirror that of the *M. truncatula ckl1/ckl2* double mutant.

REFERENCES AND NOTES

1. A. Genre, L. Lanfranco, S. Perotto, P. Bonfante, *Nat. Rev. Microbiol.* **18**, 649–660 (2020).
2. M. Parniske, *Curr. Opin. Plant Biol.* **3**, 320–328 (2000).
3. M. J. Harrison, S. Ivanov, *Curr. Opin. Plant Biol.* **38**, 101–108 (2017).
4. A. Keymer, C. Gutjahr, *Curr. Opin. Plant Biol.* **44**, 137–144 (2018).
5. P. M. Delaux, S. Schornack, *Science* **371**, eaba6605 (2021).
6. A. Bravo, T. York, N. Pumplin, L. A. Mueller, M. J. Harrison, *Nat. Plants* **2**, 15208 (2016).
7. G. V. Radhakrishnan *et al.*, *Nat. Plants* **6**, 280–289 (2020).
8. M. Menges, S. M. de Jager, W. Gruissem, J. A. H. Murray, *Plant J.* **41**, 546–566 (2005).
9. J. Lévy *et al.*, *Science* **303**, 1361–1364 (2004).
10. D. S. Floss, J. G. Levy, V. Lévesque-Tremblay, N. Pumplin, M. J. Harrison, *Proc. Natl. Acad. Sci. U.S.A.* **110**, E5025–E5034 (2013).
11. E. Gobbato *et al.*, *Curr. Biol.* **22**, 2236–2241 (2012).
12. P. Pimprikar *et al.*, *Curr. Biol.* **26**, 987–998 (2016).
13. M. J. Harrison, G. R. Dewbre, J. Liu, *Plant Cell* **14**, 2413–2429 (2002).
14. N. Pumplin, M. J. Harrison, *Plant Physiol.* **151**, 809–819 (2009).
15. G. Carotenuto *et al.*, *New Phytol.* **223**, 430–446 (2019).
16. N. Hohnjec, L. F. Czaja-Hasse, C. Hogekamp, H. Küster, *BMC Genomics* **16**, 994 (2015).
17. L. H. Luginbuehl *et al.*, *Science* **356**, 1175–1178 (2017).
18. Y. Jiang *et al.*, *Mol. Plant* **11**, 1344–1359 (2018).
19. A. Bravo, M. Brands, V. Wewer, P. Dörmann, M. J. Harrison, *New Phytol.* **214**, 1631–1645 (2017).
20. Q. Zhang, L. A. Blaylock, M. J. Harrison, *Plant Cell* **22**, 1483–1497 (2010).
21. A. Keymer *et al.*, *eLife* **6**, e29107 (2017).
22. Y. Jiang *et al.*, *Science* **356**, 1172–1175 (2017).
23. F. Feng *et al.*, *Nat. Commun.* **10**, 5047 (2019).
24. C. H. Chiu, U. Paszkowski, *Plant Physiol.* **182**, 1597–1612 (2020).
25. L. Buendia, T. Wang, A. Girardin, B. Lefebvre, *New Phytol.* **210**, 184–195 (2016).
26. G. Endre *et al.*, *Nature* **417**, 962–966 (2002).
27. S. Stracke *et al.*, *Nature* **417**, 959–962 (2002).
28. F. Maillet *et al.*, *Nature* **469**, 58–63 (2011).
29. A. Genre *et al.*, *New Phytol.* **198**, 190–202 (2013).
30. M. Venkateshwaran *et al.*, *Proc. Natl. Acad. Sci. U.S.A.* **112**, 9781–9786 (2015).
31. B. J. Sieberer, M. Chabaud, J. Fournier, A. C. Timmers, D. G. Barker, *Plant J.* **69**, 822–830 (2012).
32. E. Limpens *et al.*, *Science* **302**, 630–633 (2003).
33. L. Buendia, A. Girardin, T. Wang, L. Cottret, B. Lefebvre, *Front. Plant Sci.* **9**, 1531 (2018).
34. X. Zhang *et al.*, *Plant J.* **81**, 258–267 (2015).
35. C. Calantzis, D. Morandi, C. Arnould, V. Gianinazzi-Pearson, *Symbiosis* **30**, 97–108 (2001).
36. C. Kistner *et al.*, *Plant Cell* **17**, 2217–2229 (2005).
37. K. Demchenko, T. Winzer, J. Stougaard, M. Parniske, K. Pawlowski, *New Phytol.* **163**, 381–392 (2004).
38. E. Limpens *et al.*, *Proc. Natl. Acad. Sci. U.S.A.* **102**, 10375–10380 (2005).
39. B. Horváth *et al.*, *Mol. Plant Microbe Interact.* **24**, 1345–1358 (2011).
40. K. Yano *et al.*, *Proc. Natl. Acad. Sci. U.S.A.* **105**, 20540–20545 (2008).
41. C. Gleason *et al.*, *Nature* **441**, 1149–1152 (2006).
42. G. E. D. Oldroyd, *Nat. Rev. Microbiol.* **11**, 252–263 (2013).
43. D. Das *et al.*, *Nat. Commun.* **13**, 477 (2022).
44. J. Shi *et al.*, *Cell* **184**, 5527–5540.e18 (2021).

ACKNOWLEDGMENTS

The authors thank P. Lindsay [Boyce Thompson Institute (BTI)], F. Giska (BTI), and F. Schwanke (C. Zipfel lab, University of Zurich) for helpful discussions regarding in vitro transphosphorylation assays; P. Lindsay for advice on protein purification and coimmunoprecipitation techniques; and D. A. Daniels (BTI) for guidance on *Medicago* transformation. The BTI Computational Biology Center led by S. Strickler assembled 3′ RNA-seq and differential expression data and shared an R script for the heatmap. Confocal images were acquired using instrumentation at the BTI Plant Cell Imaging Center. The BTI Center for Plant Biotechnology Research generated *B. distachyon* transgenic plants. The authors thank D. Cook (University of California, Davis) for providing initial seed of *M. truncatula dmi2-7* and J. Vogel (Joint Genome Institute) for providing T3 seed of *B. distachyon* mutant line T-28188E. M.J.H. is affiliated with the Plant Pathology and Plant Microbe Biology Section of the School of Integrative Plant Sciences at Cornell University. **Funding:** US National Science Foundation Plant Genome Research IOS #2139351 (M.J.H.) and US National Science Foundation, Major Research Instrumentation NSF DBI-0618969 (M.J.H.). **Author contributions:** Conceptualization, Investigation, Visualization, and Data analysis: S.I. and M.J.H. Funding acquisition: M.J.H. Writing: S.I. and M.J.H. **Competing interests:** The authors declare that they have no competing interests. **Data and materials availability:** All data are available in the main text or the supplementary materials. *M. truncatula* mutants and constructs generated in this study are all available under a material transfer agreement from the Boyce Thompson Institute.

SUPPLEMENTARY MATERIALS

Submitted 27 July 2022; resubmitted 16 August 2023
Accepted 19 December 2023
10.1126/science.ade1124